Article:
Amjad, M, Gardy, J, Ali, H et al. (2018) Novel draw solution for forward osmosis based solar desalination. Applied Energy, 230. pp. 220-231. ISSN: 0306-2619

https://doi.org/10.1016/j.apenergy.2018.08.021

Novel draw solution for forward osmosis based solar desalination

Muhammad Amjad[1, 2], Jabbar Gardy[1], Ali Hassanpour[1], Dongsheng Wen[3,1*]

[1] School of Chemical and Process Engineering, University of Leeds, Leeds, LS2 9JT, UK

[2] Department of Mechanical, Mechatronics and Manufacturing Engineering (KSK Campus), University of Engineering and Technology Lahore, 54890, Pakistan.

[3] School of Aeronautic Science and Engineering, Beihang University, Beijing, 100191, P.R. China

Abstract:

Forward osmosis (FO) is an emerging technology for water desalination which requires no external force for its operation. The performance of FO for water desalination is dependent on draw solution (DS) that must provide high osmosis pressure, minimum reverse flux and efficient separation of water. This work proposes an innovative concept of energy efficient material as DS having two functions, i.e. high osmotic pressure and efficient absorption of solar energy for the regeneration phase. The potassium functionalised carbon nanofibers (K/CNF) which are highly solar absorptive, are engineered and suspended in triethylene glycol (TEG) aqueous solution with different concentrations to act as a novel DS. The TEG-K/CNF is fully characterised for morphological appearance and thermophysical characteristics before using in FO experiments. It is found that the osmotic pressure and water flux of the novel DS are directly dependent on the concentration of K/CNF and TEG. The draw solution is re-concentrated by evaporating the water aided by the highly solar absorptive K/CNF under simulated solar flux. The vapours are condensed and the quality of product water is examined and compared with portable water standard. The novel concept proposed in this study has the potential to be used in arid areas where solar energy is abundant to fulfil the potable water needs.

*Corresponding author. Tel.: 0044-113-3432678; fax: 0044-20-78825003.
Email address: d.wen@leeds.ac.uk / d.wen@buaa.edu.cn

Keywords

Forward osmosis, nanofluid, desalination, solar energy, osmotic pressure

1. Introduction

The availability of low-cost potable water has become a serious concern in the present ever-increasing world population scenario. Almost one-third of the world population is living in water stressed conditions and this figure is expected to increase to two-third in the next ten years [1]. Desalination of sea and brackish water and recycling of wastewater is being progressively practiced worldwide to augment the limited potable water supplies [2]. Easy, cost-effective and energy-efficient technologies are to be developed to cope with this ever worsening potable water issue. Using renewable energy sources, especially solar energy [3] in connection with water treatment [4, 5] and combing it with water treatment technologies [6] is highly essential in the present scenario of energy and water crisis.

Forward osmosis (FO) has recently been recognised as one of the most promising low energy technologies in the field of water desalination which uses the osmotic pressure of the draw solution to permeate portable water from the feed side through a semi-permeable FO membrane [7, 8]. Osmotically driven FO has numerous advantages over the pressure-driven reverse osmosis (RO) such as low energy intensity, less membrane fouling, minimum environmental impact of the salt concentrate, reversibility of membrane fouling, low reverse solute flux [9, 10] and water recovery up to ~70% [11, 12]. However, appropriate draw solutions (DS) for FO having high osmosis pressure, low revers flux of solute particles, easy regeneration and causing minimum membrane propensity are still to be developed to make FO a viable solution for potable water issues.

Various types of media have been experimented as FO draw solutions which can be broadly categorised as conventional DS including gas or volatile compounds [11, 13], inorganic [14,

15] and organic solutes [16, 17]. Organic coated magnetic nanoparticles (MNPs) [2, 18-21] have been used in FO draw solutions which can be regenerated using a strong electric or magnetic field followed by ultrafiltration process. Nanoparticles have the advantage of high surface area to volume ratio and larger size in comparison with ions and molecules of organic and inorganic draw solutions. Qingchun Ge *et al.* [22] investigated poly ethylene glycol di-acid coated magnetic nanoparticle [(PEG-$(COOH)_2$)-MNPs] as draw solutions but they reported aggregation of nanoparticles and water flux reduction by 21% after several runs. Ling *et al.* [23] used various concentrations of MNPs with three types of surface functional groups and observed that water flux was increased with the concentration in a non-linear manner. However there was agglomeration issue and unsatisfactory recovery of small sized MNPs due to the increased thick layer of poly acrylic acid. In another study, Ling *et al.* [24] developed poly acrylic acid (PAA) and poly(N-ispropyleacrylamide) (PNIPAM) coated MNPs with -COOH functional group. Water flux of PAA-MNPs was higher than that of PAA-PNIPAM-MNPs in either case when feed water was DI water or synthetic brackish water.

Above mentioned a few studied have shown a number of problems arising from the use of MNPs as draw solutes in FO desalination. Though these investigations are the preliminary results, they are facing the problem of agglomeration, reduced water flux over time and recovery problem of the nanoparticles even after using high magnetic field and nano filtration. Hence there is a strong prospective to develop and explore efficient nanofluid based draw solutions using other nanomaterials. Moreover, the energy aspect in the above mentioned nanoparticle based draw solutions is primarily missing. In this work we report for the first time combining FO with solar energy for water desalination using directly absorptive nanofluid.

Herein we investigate the dual functioned potassium doped carbon nanofibers (K/CNF) in tri-ethylene glycol (TEG) aqueous solution as a novel DS for producing potable water. The novel DS does not only have high osmotic pressure to develop a high water flux across the FO membrane, but also possesses a high solar absorption capability to separate product water and regenerate the draw solution. This is a unique work of its kind and utilises the solar energy for water desalination using osmotically driven forward osmosis process. Several surface treatments have been implemented to make the TEG-K/CNF composite osmotically active and a laboratory scale cross flow FO cell is used to evaluate the performance of these novel DS experimentally. The photothermal performance in water recovery phase of FO process is evaluated using simulated solar flux against various concentrations of TEG-K/CNF composite. The quality of water is examined through several water quality tests and compared with the international standards.

2. Materials and methods

2.1 Synthesis of TEG-K/CNF based draw solution

Surface functionalisation of carbon nanofiber (CNF) is an effective route where some crucial functional groups on the internal or external surface can increase the hydrophilicity. 5 g of CNF [graphitized (iron-free) compressed of conical platelets D=100 nm, L=20-200 μm, Aldrich Chemistry, USA] was immersed in an 80 mL of nitric acid:sulfuric acid (1:3, v/v) at 70 ºC for 6 h under stirring at 250 RPM. The obtained solution was then filtrated and washed several times with deionised (DI) water followed by drying in a vacuum-oven at 80 ºC overnight. The treated-CNF powder was suspended in 50 mL of 0.05 M aqueous sodium dodecyl sulfate (SDS) solution and sonicated for 30 min. Subsequently, 250 mL of 0.5 M KOH aqueous solution was added dropwise to the dispersed treated-CNF solution and the reaction mixture was then refluxed for 16 h (**Fig. 1**). After cooling, a black solution was

obtained. The as-obtained particles were separated from the solution using Megafuge at 11000 RPM and extensively washed with 1:1 of methanol to DI water until the pH of the filtrate reached a pH value of 7. The separated grey-black gel then oven-dried at 80 ºC for 24 hr and upon normalizing to room temperature it was crushed to have K/CNF powder. The measured weight K/CNF powder was dispersed in different volume concentrations of TEG to have 0.05 to 0.2 wt% concentrations. The resultant mixture was probe sonicated for 5 min to completely disperse the K/CNF in TEG aqueous solution. The synthesised TEG-K/CNF mixture was very stable even over a period of three months. The synthesis approach of TEG-K/CNF is summarised schematically in **Fig. 1**.

2.2 Characterisation techniques

The presence of functional groups in TEG-K/CNF, K/CNF and CNF samples were examined by attenuated total reflection-Fourier transform infrared (ATR-FTIR) spectroscopy at room temperature using a Nicolet iS10 FTIR spectrometer with resolution of 4 cm^{-1} (in the ranges of 500 to 4000 cm^{-1}) and the final output was in percentage transmittance. The samples of CNF, K/CNF and TEG-K/CNF were morphologically characterised using scanning electron microscopy (SEM) and transmission electron microscopy (TEM). SEM measurements were performed using a high performance cold field emission-scanning electron microscope (CFE-SEM, SU8230 Hitachi) equipped with an energy dispersive X-ray spectroscopy (EDS, Oxford INCA) to analyse the surface morphologies, location of the elements and elemental compositions of the CNF, K/CNF and TEG-K/CNF. The TEM measurements were carried out using a FEI Tecnai TF20 FEG operated at 200. Each sample was prepared separately by suspending powder in acetone, followed by ultra-sonication for 10 min. One drop of this suspension was put on a micro-copper grid covered with a thin layer of carbon for analysis.

The thermal stability of CNF, K/CNF and TEG-K/CNF samples was performed using thermo-gravimetric analysis (TGA) using the TGA/DSC-2 instrument (Mettler Toledo, England). (20±5) mg of sample was weighted in a 70 µL alumina crucible and placed on the TGA/DSC-2 sample holder. Experiment was conducted under a constant flow rate (50 mL/min) of nitrogen purge gas and the sample was heated from 30 to 900 °C at 10 °C/min. The structural characteristic of CNF, K/CNF and TEG-K/CNF samples were analysed using X-ray diffraction (XRD) on a powder Bruker's advanced D8 diffractometer using CuKα radiation (λ=1.5418 Å). The operation voltage and applied current for the XRD instrument were maintained at 40 kV and 40 mA, respectively. The samples were loaded onto the sample holder and scanned at 2θ angle range from 10 to 80^{o} with step size 0.035 at 30 sec per step. The optical absorbance of TEG-K/CNF samples was analysed with different concentrations by a UV-Vis spectrometer (UV-1800, Shimadzu) using a high precision quartz cell with light path of 10 mm. The long term stability of the sample was checked with Turbiscan (Formulaction, France) by measuring the sedimentation rate based on light backscatter and transmission measurements through the sample.

2.3 Forward osmosis (FO) setup

The performance of TEG-K/CNF as a novel draw solution (NDS) was investigated using a laboratory scale cross flow forward osmosis cell (CF042 FO, Sterlitech, USA) as shown schematically in **Fig. 2 (a)**. The FO cell has active membrane area of 42 cm^2. A pre-wetted FO flat sheet membrane (Aquaporin Inside) was used to measure the water flux of NDS against deionized water and synthetic brackish water as feed solution. The FO membrane was used in FO mode, i.e. active layer facing the feed solution (AL-FS). NDS with various concentrations of K/CNF and TEG was used to experiment the water permeation rate across the FO membrane. The water permeation was measured over a period of two hours after giving first 15 min to settle the flow fluctuations. A crossflow velocity of 8.50 cm/s was used

on both the draw side and feed side. A digital balance (AND, EK-3000I) was used to measure the weight change of the feed solution over the experiment time.

The water permeation flux (J_w) in $Lm^{-2}h^{-1}$ (known as LMH) was calculated by measuring the weight change of the feed solution over predetermined time using the following relation;

$$J_w = \frac{\Delta m}{\rho_f A \Delta t} = \frac{\Delta V}{A \Delta t} \quad (\mathbf{1})$$

where Δm is the weight change of feed solution over predetermined time (Δt), ΔV is change in volume (L) of the feed solution in time Δt (h) and A is active membrane area (m^2).

The reverse solute flux was calculated by measuring the conductivity of the feed solution at an interval of every 5 min using a calibrated conductivity meter by the following relation;

$$J_s = \frac{C_t V_t - C_o V_o}{A \Delta t} \quad (\mathbf{2})$$

where J_s is the reverse solute flux in $gm^{-2}h^{-1}$ (also known as gMH), C_o and C_t are the concentrations of the feed solution at the start of the experiment and at time Δt, respectively, V_o and V_t are the volumes of the feed solution (L) at the start and at Δt, respectively.

2.4 Setup for DS regeneration

The regeneration of the nanofluid based NDS and the product water separation was achieved through simulated solar radiation flux. A solar simulator (Newport Co.) having a class AAA certification was used as the source of simulated solar flux in this investigation. The solar simulator has a 450 W xenon lamp as the light source and spectral correction filters (known as air mass filters) to closely match the output flux with solar spectrum. An air mass filter AM1.5G was used to simulate the direct solar spectrum with the Sun at a zenith angle of 48.20 (ASTM E891). The sun simulator has a spectral match with 0.75-1.25% fraction of ideal percentage, 2% non-uniformity of irradiance and ± 2% spectral instability according to

ASTM Class AAA standard [25]. A schematic view of the experimental setup is presented in **Fig. 2 (b)**. A Fresnel lens of 5.5 x 5.5 in^2 with a focal length of 10 in was used to focus the output light onto a nanofluid sample. The focused intensity of light was measured as 10 suns with the help of a solar intensity meter.

A vessel made of high temperature quartz glass with the inner and outer diameter of 30 mm and 34 mm, respectively, was used as sample container. The vessel was put accurately under the solar radiation flux to enable a uniform heating. A sample fluid of 27 mL (~38.2 mm depth) was used to evaporate to ambience during irradiation time of 20 min. A transparent quartz cover and a condenser was integrated with the vessel to collect water vapours for a prolonged irradiation time to analyse the quality of product water. Holes of 1 mm diameter were fabricated in the vessel to insert four K-type (Omega 5TC-TT-K-36-36) thermocouples (TC) at 8, 16, 24 and 32 mm depths from the top. The uncertainty in temperature measurement was as ±0.5 °C. The data were registered by a data acquisition device (NI SCXI-1303) under the LabVIEW environment at a sampling rate of 1 Hz.

A digital balance (Ohaus, Mettler Toledo) with uncertainty of ±0.001 g was used to measure the mass change over time as the sample was radiated with solar flux. The generated steam was condensed in a glass condenser with cooling water circulating around the condensing tube as potable water for further analysis. Various weight concentrations of K/CNF were used to investigate the solar absorption for draw solution regeneration and product water recovery.

3. Results and discussion

3.1 Characterization of TEG-K/CNF material

Fig. 3 shows the ATR-FTIR spectra of CNF, K/CNF and TEG-K/CNF samples. CNF sample had almost no clear bands because the CNF acted as a very effective black body absorber [26]. In case of K/CNF and TEG-K/CNF, there were several extra characteristic peaks related

to generate functional groups on the surface as well as K-species doping into the structure of CNF as shown in **Fig. 3**. The strong broad bands at ~3150 cm^{-1} were corresponded to the –OH groups (–OH and –COOH) on the surface of CNF structure as well as the free –OH end groups of TEG structure is attached to the surface of acid treated CNF [27, 28]. The bands at ~2950 and ~2850 cm^{-1} could attribute to the asymmetric and symmetric stretching of –C-H groups, respectively, in TEG molecules functionalised CNF [29]. There were few weak peaks at ~2090 to 2390 cm^{-1} that could be assigned to the asymmetric stretching of CO_2 molecules. An additional new peak appears at ~1735 to 1750 cm^{-1} and could be related to the C=O stretching in carboxylic and carbonyl groups [26].

The band at ~1650 cm^{-1} was ascribed to the C=C stretching in the main CNF structures. The band at ~1600 cm^{-1} was corresponded to the H-O-H symmetric vibration of water molecules absorbed on the surface of K/CNF and TEG-K/CNF structures. The band at ~1440 cm^{-1} was assigned to the C-H bending of TEG groups in TEG-K/CNF. The new peak at 1350 cm^{-1} was related to the C-O stretching but the band at around 1200 cm^{-1} was assigned to the C-C stretching [29]. The sharp peak at 1060 to 1010 cm^{-1} was corresponded to the C-O bending in ether whilst the one at 840 cm^{-1} could be attributed to the –OH in carboxylic groups [26]. The intensity of this peak (at 840 cm^{-1}) in TEG-K/CNF reduced after surface functionalization with TEG [29]. This confirmed the formation of ester bond between –COOH on the surface of CNF and –OH groups of TEG molecules.

Several bands at about 765, 685, 650 and 600 cm^{-1} were attributed to the aliphatic C-H bending [30]. This result clearly indicates that the surface of K/CNF was successfully functionalised with TEG molecules. The attachment of –COOH, -OH and K groups onto the surface of CNF has a strong effect on the stability of synthesised TEG-K/CNF sample in aqueous medium and could enhance the osmotic pressure.

The morphologies of CNF, K/CNF and TEG-K/CNF samples at different magnifications are shown in **Fig. 4**. The SEM images of unmodified CNF [**Fig. 4 (a)**] at different magnifications demonstrated that the surface of CNFs was smooth and confirming the used CNF sample had short and long filled cylindrical chains of fibre covalently bonded carbon atoms which possess hydrophobic properties. The formation of the short and long filled cylindrical chains with observed channels can be attributed to the nature of the synthesis of nanofibers from different polymers.

Whereas, the morphology of K/CNF was different (roughness of the side cylindrical chains) and the carbon fibres were thicker than unmodified CNF sample. This phenomenon may be related to the surface treatment of CNF with a strong acidic mixture (H_2SO_4 and HNO_3) to form carboxylic/hydroxyl groups on the surface as well as K-species embedded in the CNF (**Fig. 4 (b)**). Having K-species doped, -COOH and –OH on the structure of CNF lead to an increase in the hydrophilicity of synthesised material which could cause an increase in the osmotic pressure. In case of TEG-K/CNF hybrid, it can be observed from **Fig. 4(c)** that there was a spongy morphology due to the surface coverage of K/CNF with TEG. This further confirms that the surface of K/CNF were successfully functionalised with TEG molecules. Addition of TEG molecules to the surface of K/CNF leads to an increase in –O– and –OH groups which would further increase the hydrophilicity of TEG-K/CNF surface.

The elemental analysis of K/CNF using SEM- EDS revealed that the synthesised K/CNF consist of carbon, oxygen and potassium elements as shown in EDS spectrum in **Fig. 5 (a)**. The K-species are evenly distributed throughout the elemental mapping (**Fig. 5 (b)**). This confirms the successful decoration of CNF with potassium in the synthesised K/CNF. The stability of the K/CNF sample was checked using Turbiscan (Formulaction, France) which measures the sedimentation rate by using turbidity measurements of backscatter and transmission to assess the stability of the sample. The transmission and backscattering spectra

as given in **Fig. 5 (c),** show no sedimentation over a period of 24 h, confirming a high stability of the sample.

The morphology of CNF and K/CNF were further investigated using TEM analysis. The TEM micrographs given in **Fig S1 and S2 in supplementary information,** proved that most of the fibres in these samples have bends and other curvature structures. The surface roughness of fibres can be seen in case of K/CNF. This was due to the doping of K-species into the structure of CNF and –COOH/–OH groups functionalising the surface of CNF.

Fig. 6 (a) presents the XRD pattern of CNF, K/CNF and TEG-K/CNF samples. It can be seen that there are two broad diffraction peaks at 2θ of 25 and 44° were corresponding to [002] and [101] in the structure of CNF, respectively [31]. It can be clearly seen that there are significant changes in the crystal structure of synthesised K/CNF and TEG-K/CNF materials in comparison with unmodified CNF. Furthermore, there was no difference between the XRD pattern of K/CNF and TEG-K/CNF samples. However, the peak intensities reduced after modification with TEG as a result of surface coverage of K/CNF with TEG molecules.

The thermal behaviours of the synthesised K/CNF and TEG-K/CNF as well as unmodified CNF sample were investigated and the corresponding TGA curves are given in **Fig 6 (b)**. It can be seen that the unmodified CNF sample was very stable and did not show any dramatic decomposition in the range of 30 to 800 °C and then only a slight weight loss could be observed. In case of K/CNF, three step of weight loss were present. The first step began at 90-140 °C possibly due to desorption of water molecules and the second one at 140-175 °C associated with the decomposition of carboxylic and hydroxyl groups on the surface of K/CNF and after 175 °C, there is almost negligible mass loss till 800 °C. The final step started at 800 °C due to the partial decomposition of CNF structure. From the mass loss it can be suggested that the CNF has been functionalised around 14 wt% with –COOH and –OH groups. In contrast, the characteristic TGA curve of TEG-K/CNF with 0.2 wt% of K/CNF

and 10 vol% TEG, exhibited a four step weight loss. There was an initial gradual mass loss, followed by a continuous weight loss (~33% over K/CNF) from 175 to 800 °C which could be attributed to the decomposition/detachment of TEG functional groups on the surface of K/CNF [29]. From the TGA analysis it can be observed that the dried TEG-K/CNF sample (solution: 10 wt% TEG and 0.2wt% K/CNF concentration) contains about 33 wt% TEG coverage on the surface of K/CNF. The adsorbed as well as free TEG in draw solution could have a direct impact on the enhanced osmotic pressure

3.2 Osmotic pressure analysis

The driving force for osmotically driven FO process is the osmotic pressure. The osmotic pressure of the NDS was measured in terms of osmolality using an osmometer (Advance Instruments, 3900) based on the principle of freezing point depression. The osmolality of samples containing various concentrations of K/CNF and TEG is presented in **Fig. 7**. The osmolality of NDS is almost linearly dependent on the concentration of novel draw solute (K/CNF, from 0.05 to 0.20 wt%) as well as TEG. The osmolality of NDS with TEG concentration from 10 to 20 vol% ranges from 1104 to 2754 mosmol/kg, which corresponds to the osmotic pressure from 28 to 70.3 bar, respectively.

The NDS in the present work are osmotically more active as compared with the other nanomaterial based FO draw solutions, yet with an innovative solar energy based easy regeneration. For example Guo et al. [32] used Na-functionalized carbon quantum dots (Na-CQDs) with a 50 wt% concentration of Na-CQDs which could develop osmotic pressure of 54.3 bar and regeneration was carried out by complex membrane distillation. Similarly, Zhao et al. [33] used up to 30 wt% of citrate coated MNPs as FO draw solution which could only develop 58.4 bar osmotic pressure to be used for protein enrichment. The NDS developed in

this work developed an osmotic pressure of 70.3 bar with a much smaller concentration of the draw solute compared to above mentioned draw solutions.

Compared with osmotic pressure of seawater which is around 26 bar [34], the osmotic pressure of the DS with K/CNF and TEG concentration of 0.2 wt% and 20 vol%, respectively, was about 70.3 bar and has the potential to desalinate seawater. The structure of TEG-K/CNF composite is enriched with hydroxyl (-OH), carboxylic (-COOH) groups and K-species, which could result in easy and increased intermolecular hydrogen bonding. The hydrogen bonding in the presence of these rich ionic species resulted in higher osmolality values [35] and thus higher water permeation flux in FO experiments.

3.3 FO performance of novel DS

The performance of NDS was investigated in terms of water permeation flux (LMH) and reverse solute flux (gMH) through a laboratory scale cross flow FO cell against deionised water and synthetic brackish water as feed solutions. The FO experiments were performed in FO mode, i.e. the active layer of the membrane facing the feed solution. The water permeation flux and reverse solute flux of NDS having various concentrations of K/CNF and TEG against DI water as feed solution are presented in **Fig. 8**. The water flux increased non-linearly with the increase in concentration of K/CNF at a given TEG volume concentration. For example, with 20 vol% of TEG, the water permeation flux increased from 10. 5 LMH to 13.3 LMH as the concentration of K/CNF was increased from 0.05 to 0.2 wt%, respectively. This is because the increasing concentration of K/CNF causes an increase in the net osmotic driving force. The concentration of TEG also enhances the water flux for a given concentration of K/CNF because of its hydrophilic nature. For a concentration of 0.2 wt% of K/CNF, the water flux was increased from 7.5 to 13.3 LMH when the volume concentration of TEG was increased from 10 to 20 vol%, respectively. The presence of hydroxyl and

carboxylic functional groups in TEG-K/CNF hybrid made them highly hydrophilic and thus increased water flux across the membrane.

Several investigations used magnetic nanoparticles (MNPs) with different coating agents to evaluate their performance in FO process. For example, Bai et al. [36] investigated dextran coated MNPs based draw solution where they used about 78 wt% dextran in the solution and could only achieved a water flux of about 4 LMH with DI water as feedstock, Na et al. [37] experimented citrate coated MNP with 48.5 wt% concentration of sodium citrate and observed a water flux of 6.2 LMH in first 5min of FO operation which was exponentially declined with time. Similarly, Ge et al. [22] observed a water flux of 9 LMH in first 30 min using PEG coated MNPs and Ling et al. [23] achieved 7.7 LMH with PAA coated MNPs with DI water as a feed solution. Compared with the above mentioned coated MNPs in FO process and their complexity and deteriorating performance during regeneration under strong magnetic field, the novel draw solution in the present work only contained maximum of 20 vol% TEG and developed a water flux of 13.3 LMH.

The water flux of NDS was compared with that of a widely used model FO draw solute, sodium chloride with 1.0 M concentration. As shown in **Fig. 8**, the water flux for 1.0 M NaCl draw solution was around 7.4 LMH which is almost equal to that of 0.05 wt% K/CNF in 15 vol% TEG. With this much of water flux, if the solute leakage (J_s) across the membrane is considered, it can be seen from **Fig. 8** that the reverse solute flux for 1.0 M NaCl as DS was 4.2 gMH while it is only 0.25 gMH for the TEG-K/CNF draw solution. The maximum experimental reverse solute flux for the NDS was even less than 0.5 gMH. A very lower value of J_s in case of TEG-K/CNF draw solution shows a strong binding between the K, CNF and TEG which suppressed solute diffusion across the membrane. The reverse solute flux results in membrane fouling and a decline in water flux in long term operations as well as loss of draw solution [38].

The ratio of reverse solute flux to water flux (J_s/J_w) is known as specific solute flux and is one of the most important parameters to judge the performance of FO process. The specific solute flux (gL^{-1}) is the amount of solute leakage from the draw side to the feed side for one litre of water permeation. The specific solute flux in case of 1.0 M NaCl as DS was 0.56 g/L while it is only 0.031 g/L for the maximum concentration of TEG-K/CNF draw solution within the domain of this work which is negligibly small. Very small value of specific solute flux for the NDS implies its long term operation in the FO process.

The FO performance of the novel draw solution was also checked against synthetic brackish water containing 3.0 wt% NaCl solution as feed water. **Fig. 9 (a)** shows the water flux at different TEG-K/CNF concentrations against synthetic water as feed solution. Though, the water permeation flux is reduced with NaCl solution as feed water but still the novel DS have enough osmotic force to produce a water flux of 5.7 LMH at a K/CNF concentration of only 0.05 wt% in 20 vol% TEG aqueous solution. A water flux of 8.6 LMH was observed with 0.2 wt% K/CNF concentration when TEG was 20 vol% in the draw solution and 3.0 wt% NaCl solution as feed water indicating that the NDS was still osmotically strong enough in the domain of this work to desalinate brackish with even higher salinity level.

Fig. 9 (b) shows the FO performance of the novel DS with concentrations of 0.2 wt% and 20 vol% of K/CNF and TEG, respectively over 5 runs with DI water as feed solution. The diluted DS after every cycle was concentrated by evaporating the water to bring it back to the original concentration. The water flux of 13.3 LMH was observed in first run and then though, there was a slight decline to 12.9 LMH for the fifth run. This slight decline in water flux might be due to a little change in the draw solution concentration when water was evaporated in the evaporation phase. A very small decline in water flux over the five runs shows the suitability for long term performance of the NDS.

3.4 Photothermal performance and DS regeneration

Draw solution regeneration and product water recovery is the second phase in FO desalination. The NDS did not only developed a high osmotic pressure and thus enhanced water flux across the FO membrane but was also highly absorptive of the solar radiation flux.

Fig. 10 (a) shows the temperature variation in 1.0 M NaCl solution sample and **Fig. 10 (b)** shows the temperature change in NDS sample containing only 0.2 wt% solar absorptive K/CNF and 10 vol% TEG, when exposed to radiation flux for 20 min. It could be seen that the temperature distribution was almost uniform along the optical depth of the salt solution sample (**Fig. 10 (a)**). Most of the radiation flux passed through the sample volume due to its very poor solar absorption and transparent nature. Whereas, there was a clear non-uniform temperature distribution in case of NDS sample and the rate of rise in temperature at a depth 8 mm (surface temperature) was much higher than that of lower depths (**Fig. 10 (b)**). The clear non-uniform temperature distribution along the optical depth of the NDS sample showed that most of the radiation energy was absorbed at the surface due to highly absorptive nature of the sample.

The water flux based on the change in mass of the samples over the irradiation time is given in **Fig. 11**. With salt solution sample, a water flux of even less than 1.0 LMH was achieved because water and salt contents had poor solar absorption capability and the radiations passed through the sample volume due to their transparent nature, thereby increasing the temperature very slowly from the bottom. On the other hand, the water flux ranges in three to four folds in case of NDS with concentrations in the experimental domain of this work as compared to 1.0 M NaCl solution presented in **Fig. 11**.

The water flux increased linearly with the concentration of K/CNF for a given volume concentration of TEG. For example, for 20 vol% of TEG, water flux increased from 3.02 to

3.84 LMH when the K/CNF concentration was increased from 0.05 to 0.2 wt%, respectively. This enhancement was associated with increased photo absorptivity of the NDS sample with K/CNF concentration. The radiations were absorbed at the surface layer thereby increasing the temperature (**Fig. 10 (b)**) and resulting in more evaporation from the liquid surface layer. With the increase in K/CNF concentration, the ability to absorb radiation flux was increased which resulted in higher evaporation of the liquid from the top surface for a given TEG volume concentration.

However, the vapour generation and thus the water flux was slightly reduced when TEG concentration was increased from 10 to 20 vol% for a given K/CNF concentration. For 0.05 wt% concentration of K/CNF, the water flux was slightly decreased from 3.40 to 3.02 LMH when TEG concentration was increased from 10 to 20 vol% respectively. This slight decline in water flux was associated with a relatively lowered water potential with increased TEG concentration in the solution. Moreover, the difference in water flux between the two steps of the FO solar desalination process i.e. FO step and regeneration step, could be balanced by carefully selecting the surface area of the sample container for a given solar intensity.

In addition to temperature distribution and water flux, photothermal performance was also analysed in terms of photothermal conversion efficiency (PTE) and its enhancement over 1.0 M NaCl solution. **Fig. 12 (a)** shows the photothermal efficiency and **Fig. 12 (b)** presents the PTE enhancement. PTE was calculated using the following relation [39];

$$\eta_{PTC} = \frac{c_p \sum_{i=1}^{n}(m_i \Delta T_i) + \int_0^t L_v m_v dt}{\int_0^t I A_a dt} \quad \textbf{(3)}$$

where c_p, m and ΔT are the specific heat capacity, mass of the sample taken and temperature change of the fluid volume over the specified time (dt). I is the solar irradiance, A_a is the area of the aperture, L_v is the latent heat of vaporization of water and m_v is mass of the condensed vapors in time dt.

PTE includes both the components of heat, i.e. sensible heat, as well as latent heat absorbed by the sample during the irradiation time. PTE for 1.0 M NaCl sample was observed to be 39% while it was related almost linearly with the K/CNF concentration for a given volume concentration of TEG in case of NDS. PTE increased from 65 to 77% when the K/CNF concentration was increased from 0.05 to 0.20 wt% with 20 vol% TEG concentration. This increase in PTE was associated with enhanced solar absorption capability of the sample with increased K/CNF concentration. In addition, the extinction effect of the sample was also increased meaning the colour became darker with increased K/CNF concentration and thus most of the radiations were absorbed instead of passing through the sample which was also verified from the UV-Vis spectra as shown in **Fig. S3 in supplementary information**.

However, PTE was slightly decreased with an increase in the concentration of TEG for a given K/CNF concentration. Photothermal efficiency was decreased from 69 to 65% when the TEG concentration was increased from 10 to 20 vol%, respectively, with 0.05 wt% K/CNF concentration. Similarly with 0.20 wt% K/CNF, PTE decreased from 80 to 76% when TEG concentration was increased from 10 to 20 vol% as given in **Fig. 12 (a)**. The reason of a slight decrease in PTE with increasing TEG concentration was thought of the decrease in water contents and also the coverage of K/CNF surface in the presence of TEG which can also be verified from the optical absorbance spectra (**Fig. S4 in supplementary information)** where the absorbance was slightly decreased with the increase in TEG volume concentration in the sample. Furthermore, the boiling temperature of TEG is almost three times higher that of water, hence more energy is required to detach water molecules from TEG molecules. An increase in the concentration of TEG in the mixture definitely increased water flux in FO phase but it had a little negative effect in the regeneration phase of FO process. Therefore, this small suppression of photothermal performance (~4%) can be compromised over the

corresponding higher enhancement in osmotic pressure (~150%) with an increase in TEG concentration.

The enhancement in PTE is given in **Fig. 12 (b)** which is a further elaboration of the effect of K/CNF and TEG concentrations on the photothermal performance of NDS in regeneration phase of FO process. Compared with 1.0 M salt solution, an enhancement of 105% was observed with 0.20 wt% K/CNF in 10 vol% TEG. The osmotic pressure and thus water permeation flux was amplified with increased concentration of both K/CNF and TEG in the first phase of FO process. However, the higher concentration of TEG slightly suppressed the photothermal performance of NDS in the second phase, i.e. regeneration.

3.5 Product water quality analysis

The quality of the product water was analysed by measuring pH, total dissolved solids (TDS) and turbidity. The absorbance and transmittance spectra from UV-Vis spectrometer and FTIR, respectively were also compared to see any difference between DI water and product water and to examine the presence of TEG and/or K/CNF traces. The pH and TDS of the product water were 6.2 and 22 mg/L which were within the acceptable range prescribed by WHO [40]. The turbiscan spectra for transmission and backscattering of the product water sample and DI water were exactly overlapping as shown in **Fig. S5 in Supplementary information**, showing the same turbidity. **Fig. 13 (a)** shows the FTIR spectra of the product water sample and DI water which were overlapping showing the absence of any TEG in the product water. Similarly **Fig. 13 (b)** shows the UV-Vis spectra of the product water and DI water samples further confirming that the product does not containing any of K/CNF or TEG traces.

4. Conclusions

A novel draw solution (NDS), capable of producing high osmotic pressure and direct solar absorption has been developed and tested. The dual functioned TEG-K/CNF based NDS synthesised in this study possessed high osmosis pressure which is suitable for FO and exhibited efficient direct solar absorption which is ideal for their regeneration step. The conclusions can be summarized as follows;

- The TEG-K/CNF being rich in osmotically active species, exhibited high osmotic pressure and thus led to a higher water flux in the FO experiment. With K/CNF and TEG concentrations of 0.2 wt% and 20 vol%, an osmolality of 2755 mosmol/kg was observed corresponding to an osmotic pressure of 70.3 bar.
- The FO performance of the NDS was experimentally investigated against DI water and 3.0 wt% NaCl solution as the model feed water, using a cross flow FO cell and an asymmetric FO membrane with its active side facing feed solution (FO mode). The proposed novel DS (0.2 wt% concentration in 20 vol% TEG aqueous solution) exhibited a water flux of 13.3 LMH which is almost 80% higher than that of 1.0 M NaCl solution when DI water was used as the feed solution.
- The specific solute flux with the maximum concentration of TEG-K/CNF within the domain of this work was 0.031 g/L which is negligible as compared to 1.0 M NaCl as DS. Moreover, the performance of novel DS was consistent over five runs which showed its potential for longer FO operation.
- The DS regeneration was accomplished with a simulated solar flux. There was an enhancement of 105% in the photothermal efficiency with K/CNF and TEG concentrations of 0.20 wt% and 10 vol%. At higher concentrations of TEG the photothermal performance of NDS was slightly supressed (~4%), but that was almost

negligible as compared to a significant enhancement in osmotic pressure (~150%) and water permeation flux in the first phase of FO process.

- The quality of product water was evaluated by measuring the pH, TDS, turbidity, FTIR and UV-Vis spectra and the results were within the range of potable water quality standards.
- The consistent FO performance, enhanced direct solar absorption and quality of product water demonstrated the new draw solutions developed in this work could be a potential candidate for the solar assisted forward osmosis desalination process.

Acknowledgement

The authors acknowledge the financial support from University of Engineering and Technology Lahore, Pakistan under Faculty Development Program, and 111 project (B18002) from State Administration of Foreign Experts Affairs, P.R. China..

Conflicts of interest

The authors declare no conflict of interest.

References

1. Dey, P. and E.L. Izake, *Magnetic nanoparticles boosting the osmotic efficiency of a polymeric FO draw agent: Effect of polymer conformation.* Desalination, 2015. 373: p. 79-85.
2. Dey, P. and E.L. Izake, *Mixed Polymer-Coated Magnetic Nanoparticles as Forward Osmosis Draw Agents of Tuned Hydrophilicity.* Chemistry – A European Journal, 2016. 22(32): p. 11253-11260.
3. Zhang, M., C. Xu, X. Du, M. Amjad, and D. Wen, *Off-design performance of concentrated solar heat and coal double-source boiler power generation with thermocline energy storage.* Applied Energy, 2017. 189: p. 697-710.

4. Zeng, J. and Y. Xuan, *Enhanced solar thermal conversion and thermal conduction of MWCNT-SiO2/Ag binary nanofluids.* Applied Energy, 2018. 212: p. 809-819.

5. Wang, X., Y. He, X. Liu, G. Cheng, and J. Zhu, *Solar steam generation through bio-inspired interface heating of broadband-absorbing plasmonic membranes.* Applied Energy, 2017. 195: p. 414-425.

6. Liu, X., X. Wang, J. Huang, G. Cheng, and Y. He, *Volumetric solar steam generation enhanced by reduced graphene oxide nanofluid.* Applied Energy, 2018. 220: p. 302-312.

7. Wei, R., S. Zhang, Y. Cui, R.C. Ong, T.-S. Chung, B.J. Helmer, and J.S. de Wit, *Highly permeable forward osmosis (FO) membranes for high osmotic pressure but viscous draw solutes.* Journal of Membrane Science, 2015. 496: p. 132-141.

8. McCutcheon, J.R., R.L. McGinnis, and M. Elimelech, *Desalination by ammonia–carbon dioxide forward osmosis: Influence of draw and feed solution concentrations on process performance.* Journal of Membrane Science, 2006. 278(1–2): p. 114-123.

9. Altaee, A., G. Zaragoza, and H.R. van Tonningen, *Comparison between Forward Osmosis-Reverse Osmosis and Reverse Osmosis processes for seawater desalination.* Desalination, 2014. 336: p. 50-57.

10. Field, R.W. and J.J. Wu, *Mass transfer limitations in forward osmosis: Are some potential applications overhyped?* Desalination, 2013. 318: p. 118-124.

11. McGinnis, R.L., N.T. Hancock, M.S. Nowosielski-Slepowron, and G.D. McGurgan, *Pilot demonstration of the NH3/CO2 forward osmosis desalination process on high salinity brines.* Desalination, 2013. 312: p. 67-74.

12. Coday, B.D., P. Xu, E.G. Beaudry, J. Herron, K. Lampi, N.T. Hancock, and T.Y. Cath, *The sweet spot of forward osmosis: Treatment of produced water, drilling wastewater, and other complex and difficult liquid streams.* Desalination, 2014. 333(1): p. 23-35.

13. Sato, N., Y. Sato, and S. Yanase, *Forward osmosis using dimethyl ether as a draw solute.* Desalination, 2014. 349: p. 102-105.

14. Roy, D., M. Rahni, P. Pierre, and V. Yargeau, *Forward osmosis for the concentration and reuse of process saline wastewater.* Chemical Engineering Journal, 2016. 287: p. 277-284.

15. Ge, Q., F. Fu, and T.-S. Chung, *Ferric and cobaltous hydroacid complexes for forward osmosis (FO) processes.* Water Research, 2014. 58: p. 230-238.

16. Nguyen, H.T., N.C. Nguyen, S.-S. Chen, H.H. Ngo, W. Guo, and C.-W. Li, *A new class of draw solutions for minimizing reverse salt flux to improve forward osmosis desalination.* Science of The Total Environment, 2015. 538: p. 129-136.

17. Zhao, P., B. Gao, Q. Yue, J. Kong, H.K. Shon, P. Liu, and Y. Gao, *Explore the forward osmosis performance using hydrolyzed polyacrylamide as draw solute for dye wastewater reclamation in the long-term process.* Chemical Engineering Journal, 2015. 273: p. 316-324.

18. Mino, Y., D. Ogawa, and H. Matsuyama, *Functional magnetic particles providing osmotic pressure as reusable draw solutes in forward osmosis membrane process.* Advanced Powder Technology, 2016. 27(5): p. 2136-2144.

19. Park, S.Y., H.-W. Ahn, J.W. Chung, and S.-Y. Kwak, *Magnetic core-hydrophilic shell nanosphere as stability-enhanced draw solute for forward osmosis (FO) application.* Desalination, 2016. 397: p. 22-29.

20. Zhao, Q., N. Chen, D. Zhao, and X. Lu, *Thermoresponsive Magnetic Nanoparticles for Seawater Desalination.* ACS Applied Materials & Interfaces, 2013. 5(21): p. 11453-11461.

21. Ge, Q., L. Yang, J. Cai, W. Xu, Q. Chen, and M. Liu, *Hydroacid magnetic nanoparticles in forward osmosis for seawater desalination and efficient regeneration via integrated magnetic and membrane separations.* Journal of Membrane Science, 2016. 520: p. 550-559.

22. Ge, Q., J. Su, T.-S. Chung, and G. Amy, *Hydrophilic Superparamagnetic Nanoparticles: Synthesis, Characterization, and Performance in Forward Osmosis Processes.* Industrial & Engineering Chemistry Research, 2011. 50(1): p. 382-388.

23. Ling, M.M., K.Y. Wang, and T.-S. Chung, *Highly Water-Soluble Magnetic Nanoparticles as Novel Draw Solutes in Forward Osmosis for Water Reuse.* Industrial & Engineering Chemistry Research, 2010. 49(12): p. 5869-5876.

24. Ling, M.M. and T.-S. Chung, *Surface-Dissociated Nanoparticle Draw Solutions in Forward Osmosis and the Regeneration in an Integrated Electric Field and Nanofiltration System.* Industrial & Engineering Chemistry Research, 2012. 51(47): p. 15463-15471.

25. Amjad, M., H. Jin, X. Du, and D. Wen, *Experimental photothermal performance of nanofluids under concentrated solar flux.* Solar Energy Materials and Solar Cells, 2018. 182: p. 255-262.

26. Zhou, J.-H., Z.-J. Sui, J. Zhu, P. Li, D. Chen, Y.-C. Dai, and W.-K. Yuan, *Characterization of surface oxygen complexes on carbon nanofibers by TPD, XPS and FT-IR.* Carbon, 2007. 45(4): p. 785-796.

27. Van Thu, L., N. Cao Long, L. Quoc Trung, N. Trinh Tung, N. Duc Nghia, and V. Minh Thanh, *Surface modification and functionalization of carbon nanotube with some organic compounds.* Advances in Natural Sciences: Nanoscience and Nanotechnology, 2013. 4(3): p. 035017.

28. Massoumi, B., V. Badr-Valizad, and M. Jaymand, *In situ chemical oxidative graft polymerization of aniline from phenylamine end-caped poly(ethylene glycol)-functionalized multi-walled carbon nanotubes.* RSC Advances, 2015. 5(51): p. 40840-40848.

29. Baykal, A., S. Güner, and A. Demir, *Synthesis and magneto-optical properties of triethylene glycol stabilized Mn1−xZnxFe2O4 nanoparticles.* Journal of Alloys and Compounds, 2015. 619: p. 5-11.

30. D. Pavia, G.L., G. Kriz, J. Vyvyan, *Introduction to Spectroscopy.* 2008.

31. Lee, H.-M., H.-R. Kang, K.-H. An, H.-G. Kim, and B.-J. Kim, *Comparative studies of porous carbon nanofibers by various activation methods.* Carbon letters, 2013. 14(3): p. 180-185.

32. Guo, C.X., D. Zhao, Q. Zhao, P. Wang, and X. Lu, *Na(+)-functionalized carbon quantum dots: a new draw solute in forward osmosis for seawater desalination.* Chem Commun (Camb), 2014. 50(55): p. 7318-21.

33. Zhao, D., S. Chen, C. Guo, Q. Zhao, and X. Lu, *Multi-functional Forward Osmosis Draw Solutes for Seawater Desalination.* Chinese Journal of Chemical Engineering, 2016.

34. Ge, Q., M. Ling, and T.-S. Chung, *Draw solutions for forward osmosis processes: Developments, challenges, and prospects for the future.* Journal of Membrane Science, 2013. 442: p. 225-237.

35. Świergiel, J. and J. Jadżyn, *Structure of hydrogen bonded supramolecular self-assembles controlled by the structure of monomers: 1,1- and 1,3-diethylureas.* Reactive and Functional Polymers, 2016. 105: p. 129-133.

36. Bai, H., Z. Liu, and D.D. Sun, *Highly water soluble and recovered dextran coated Fe3O4 magnetic nanoparticles for brackish water desalination.* Separation and Purification Technology, 2011. 81(3): p. 392-399.

37. Na, Y., S. Yang, and S. Lee, *Evaluation of citrate-coated magnetic nanoparticles as draw solute for forward osmosis.* Desalination, 2014. 347: p. 34-42.

38. Qasim, M., F. Mohammed, A. Aidan, and N.A. Darwish, *Forward osmosis desalination using ferric sulfate draw solute.* Desalination, 2017. 423: p. 12-20.

39. Amjad, M., G. Raza, Y. Xin, S. Pervaiz, J. Xu, X. Du, and D. Wen, *Volumetric solar heating and steam generation via gold nanofluids.* Applied Energy, 2017. 206: p. 393-400.

40. WHO, *Guidelines for drinking-water quality*. 2017, World Health Organization, Switzerland.

List of figures

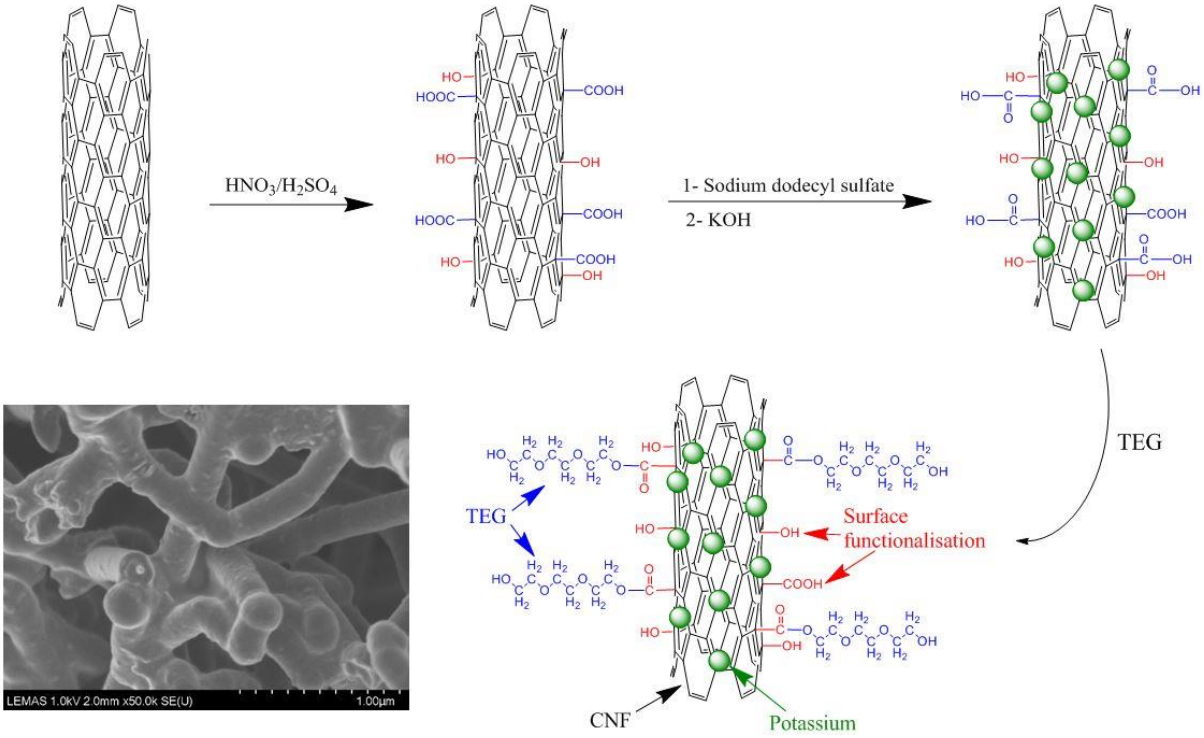

Fig. 1 The schematic synthesis route of TEG-K/CNF novel draw solution

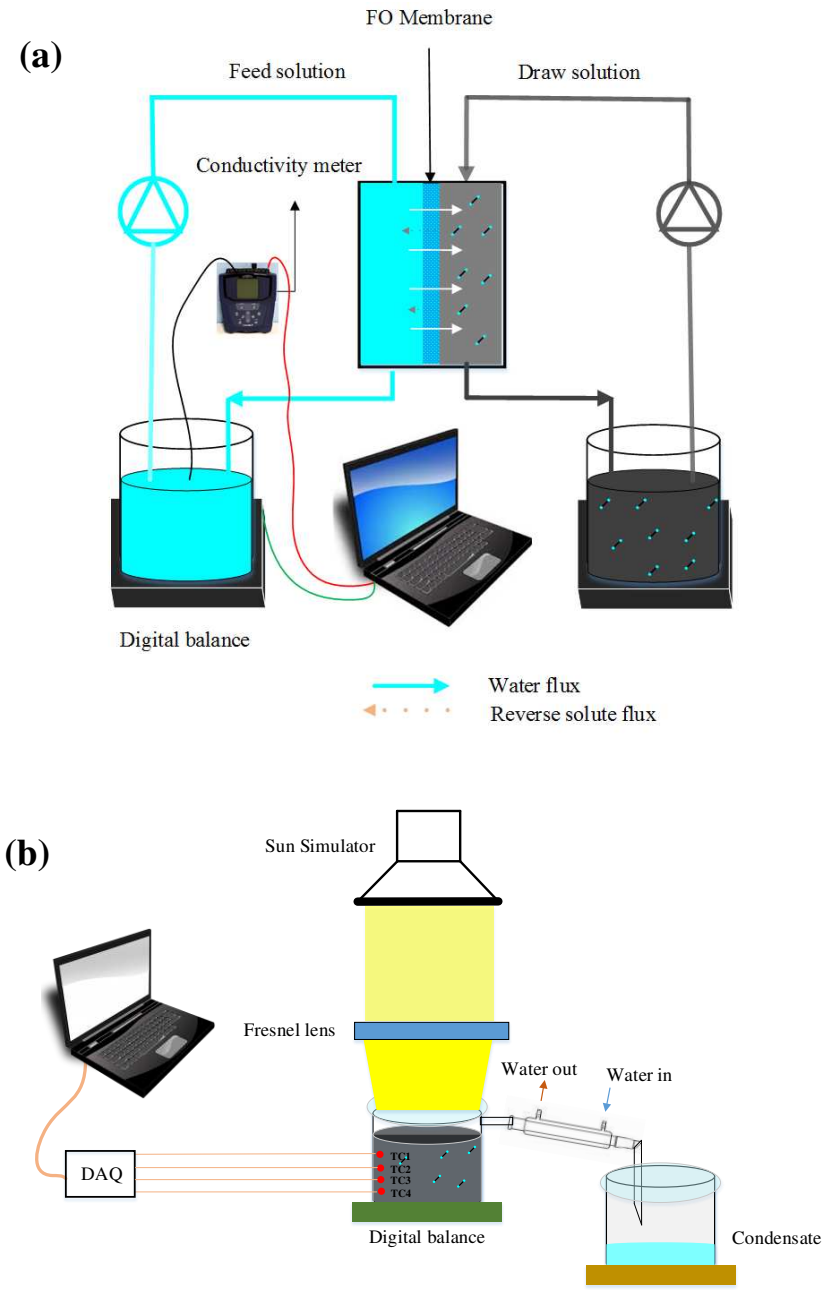

Fig. 2 Schematic of the experimental (a) laboratory scale FO setup for the investigation of water flux and reverse solute flux, and (b) setup for photothermal performance and draw solution regeneration

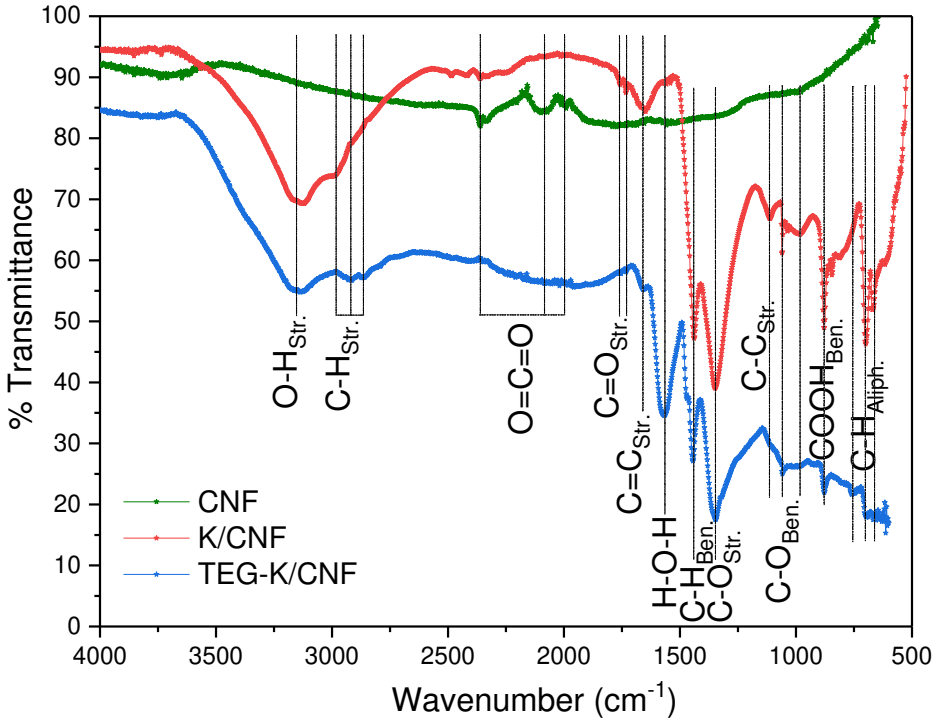

Fig. 3 FTIR spectra for CNF, K/CNF and TEG-K/CNF samples

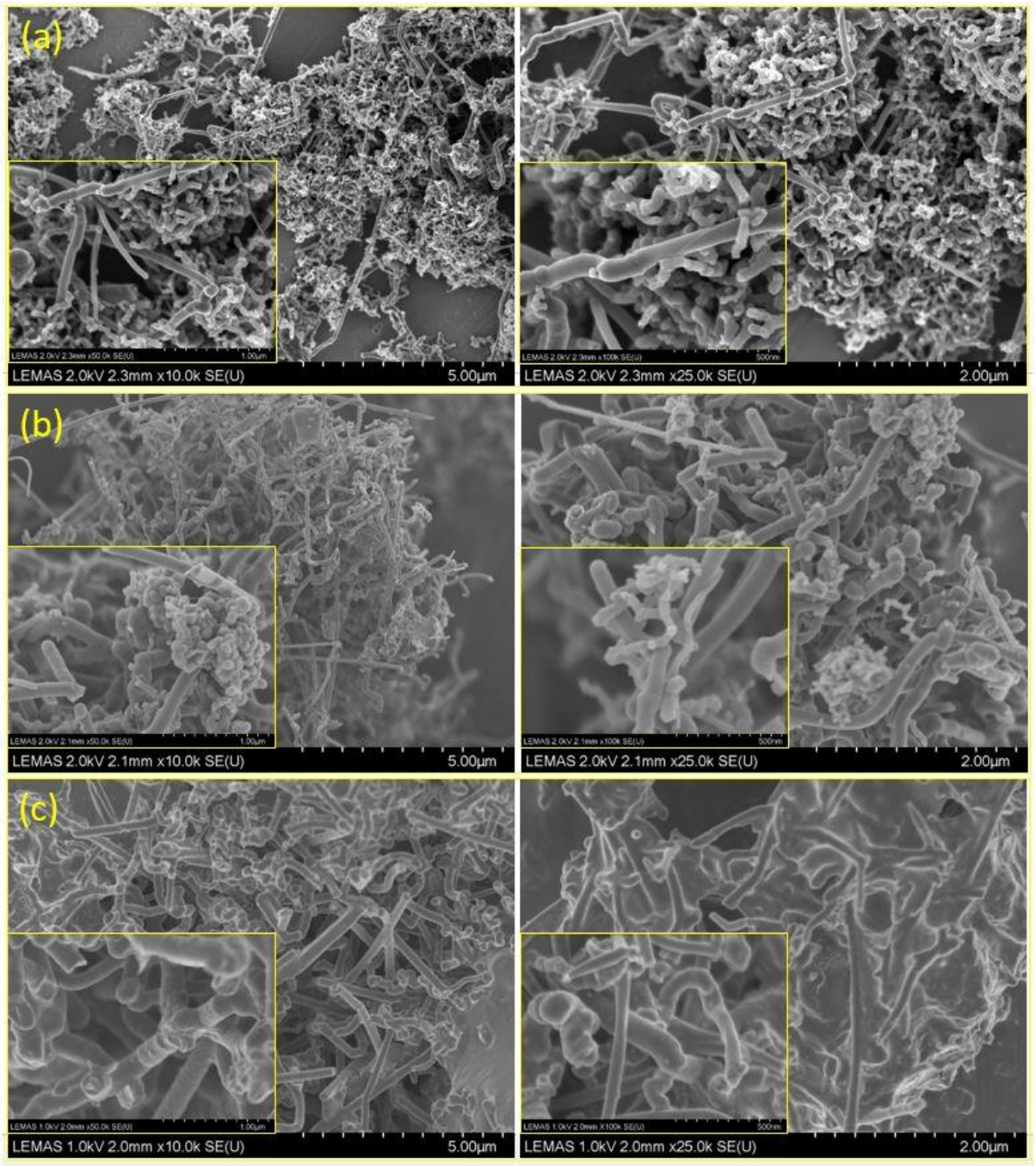

Fig. 4 SEM micrograms for (a) CNF, (b) K/CNF and (c) TEG-K/CNF at different magnifications

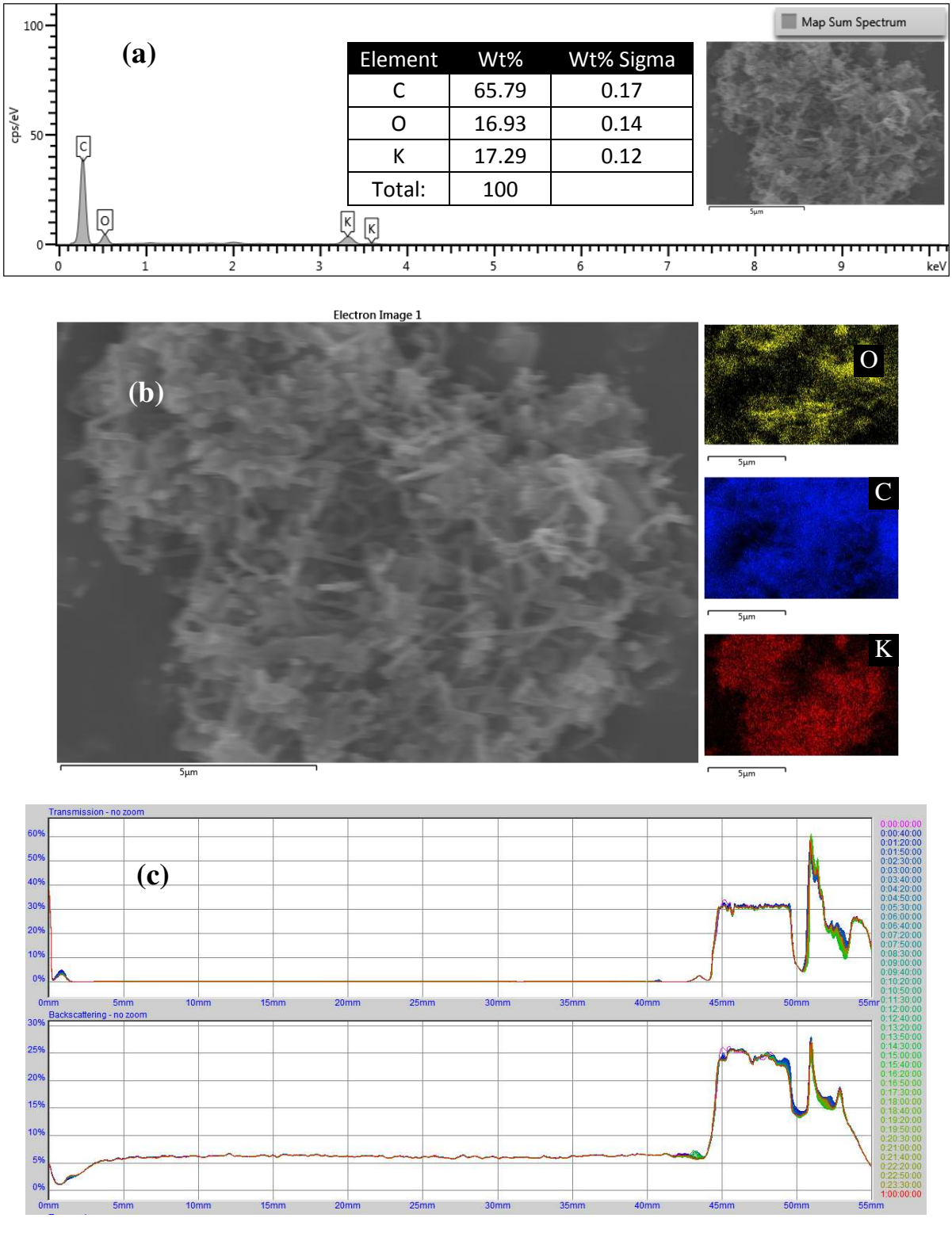

Fig. 5 (a) SEM-EDS spectrum showing the elemental composition, (b) EDS-mapping of K/CNF sample and (c) Transmission and backscattering spectra of Turbiscan over a period of 24 hours showing a very good stability

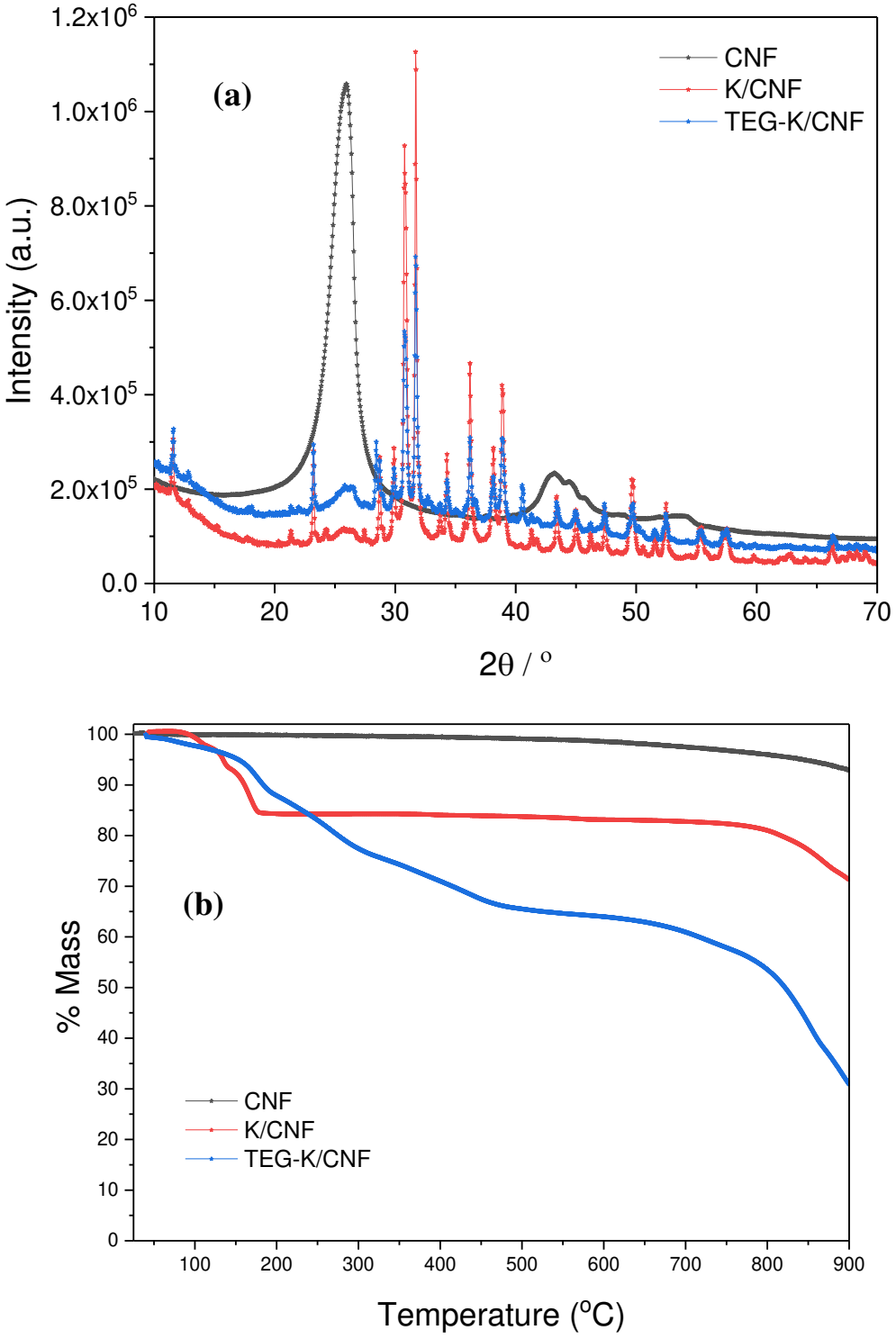

Fig. 6 (a) XRD profiles at room temperature and (b) TGA curves for CNF, K/CNF and TEG-K/CNF samples

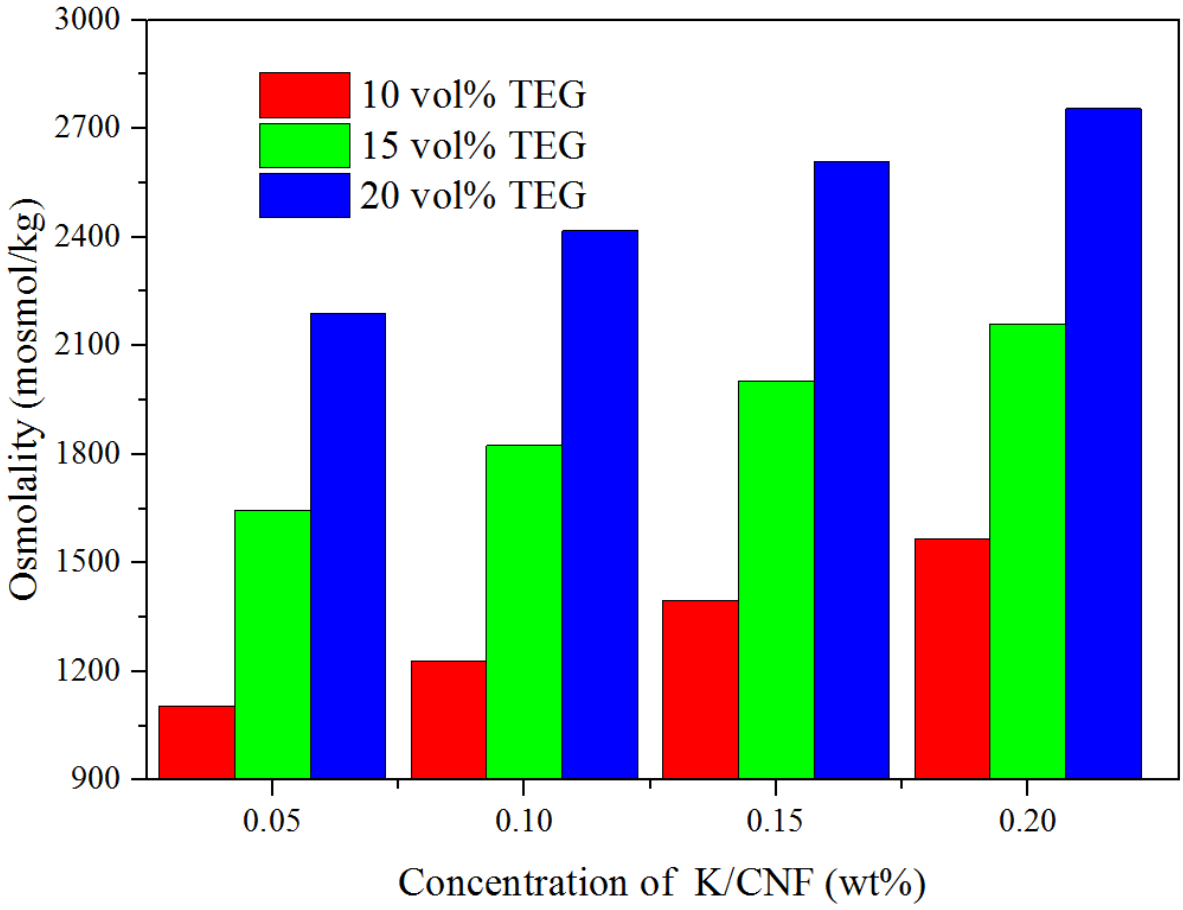

Fig. 7 Osmotic pressure in terms of osmolality of the novel DS at various concentrations

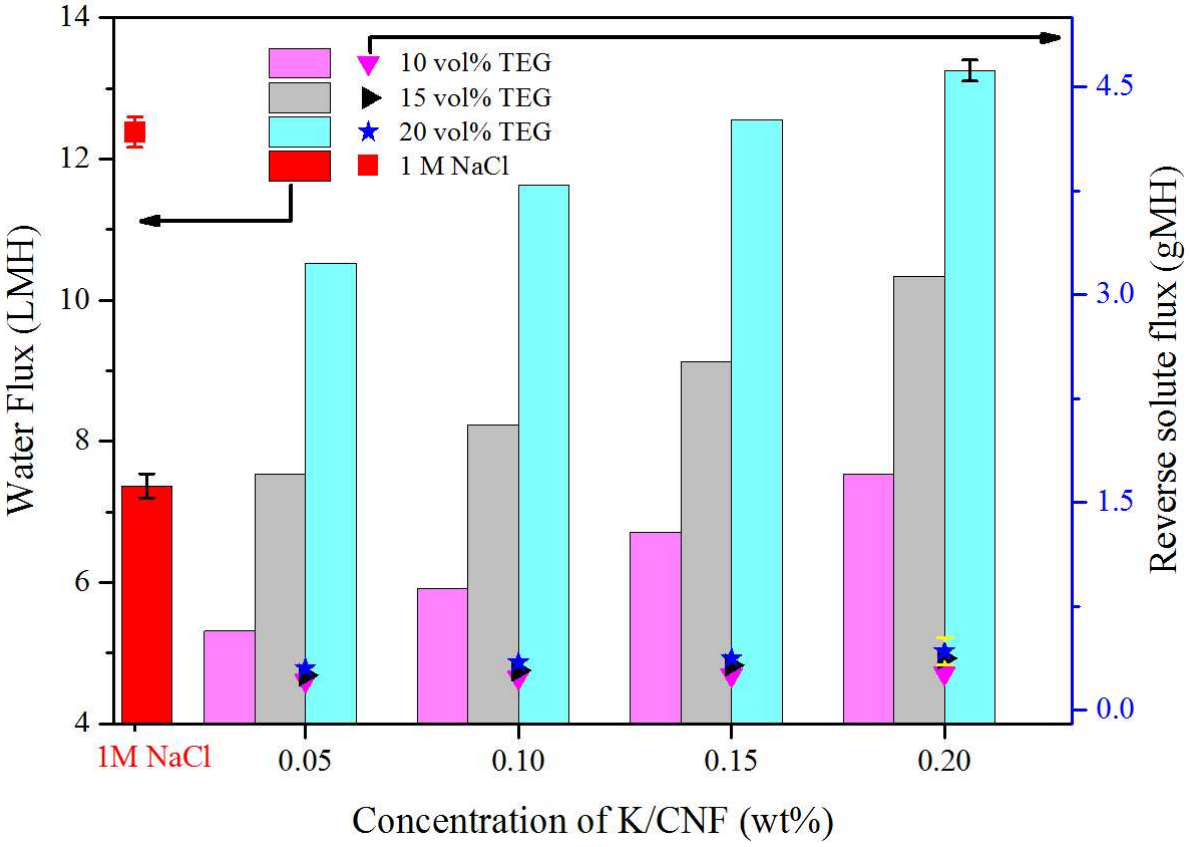

Fig. 8 Water flux and reverse solute flux against various concentrations of K/CNF and TEG with DI water as feed solution.

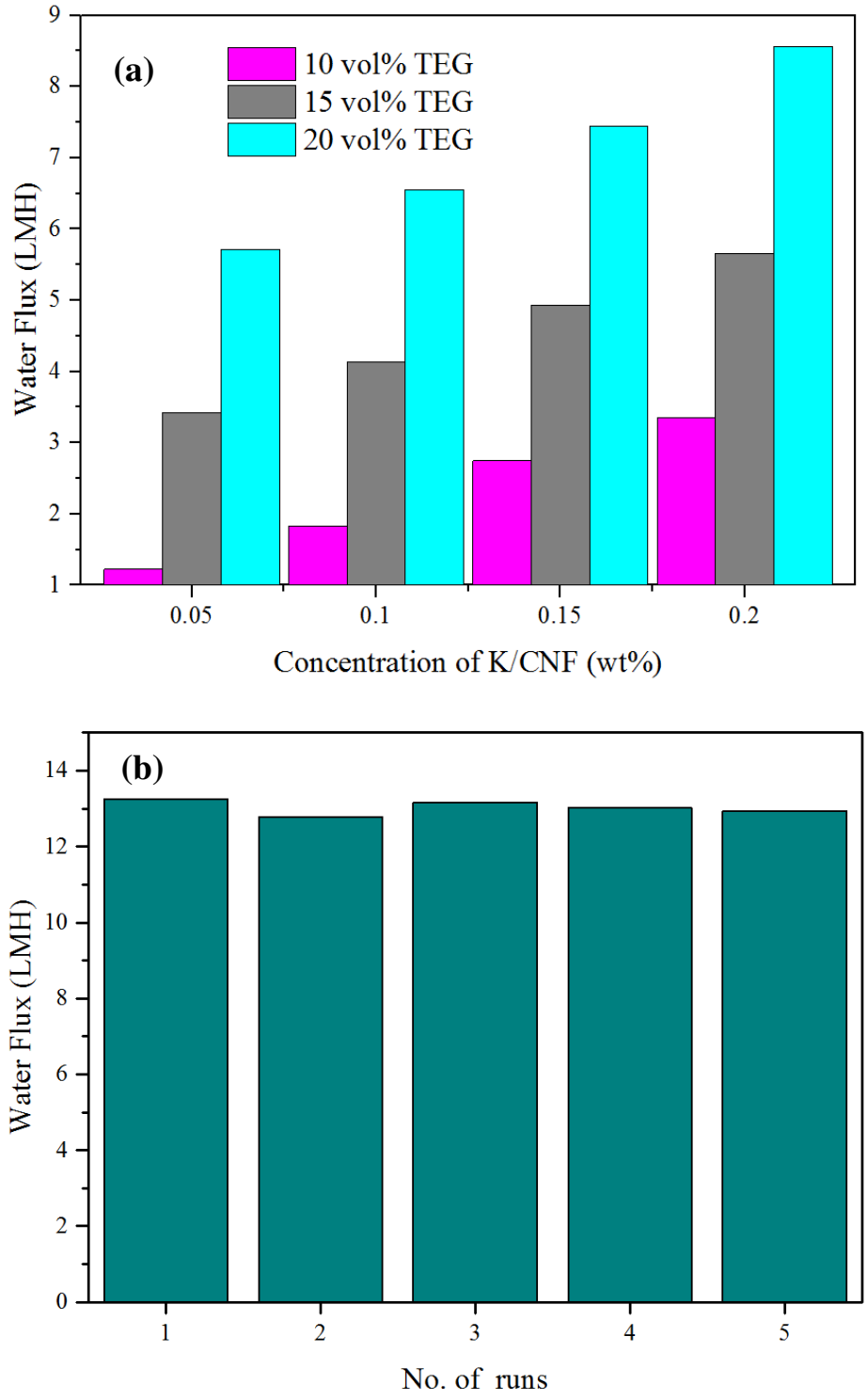

Fig. 9 FO performance of novel draw solution at various concentration with synthetic brackish water (3 wt% NaCl solution) as feed solution, (b) performance of NDS having 0.2 wt% K/CNF in 20 vol% TEG concentration over five runs

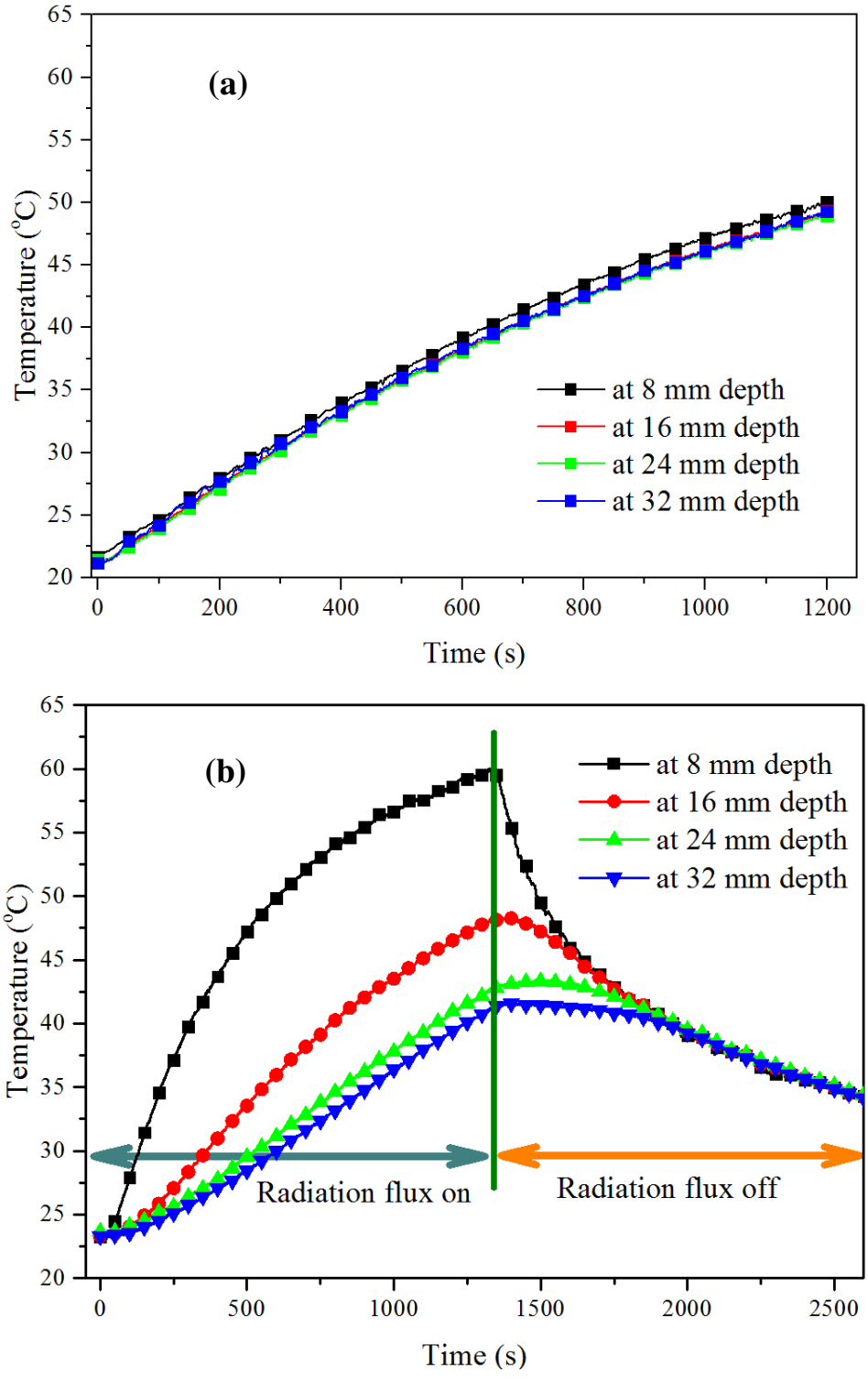

Fig. 10 (a) Temperature distribution along the optical depth of (a) 1.0 M NaCl and (b) NDS with 0.2 wt% in 10 vol% TEG when radiated under a flux of 10 suns

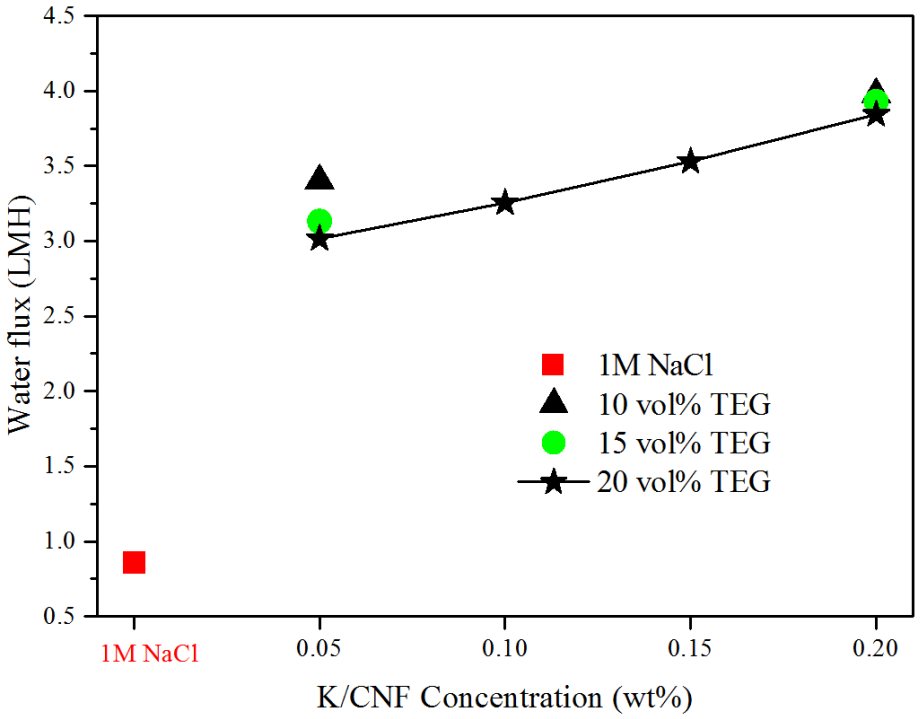

Fig. 11 Water flux of NDS with various concentrations of K/CNF and TEG in the regeneration phase of FO process

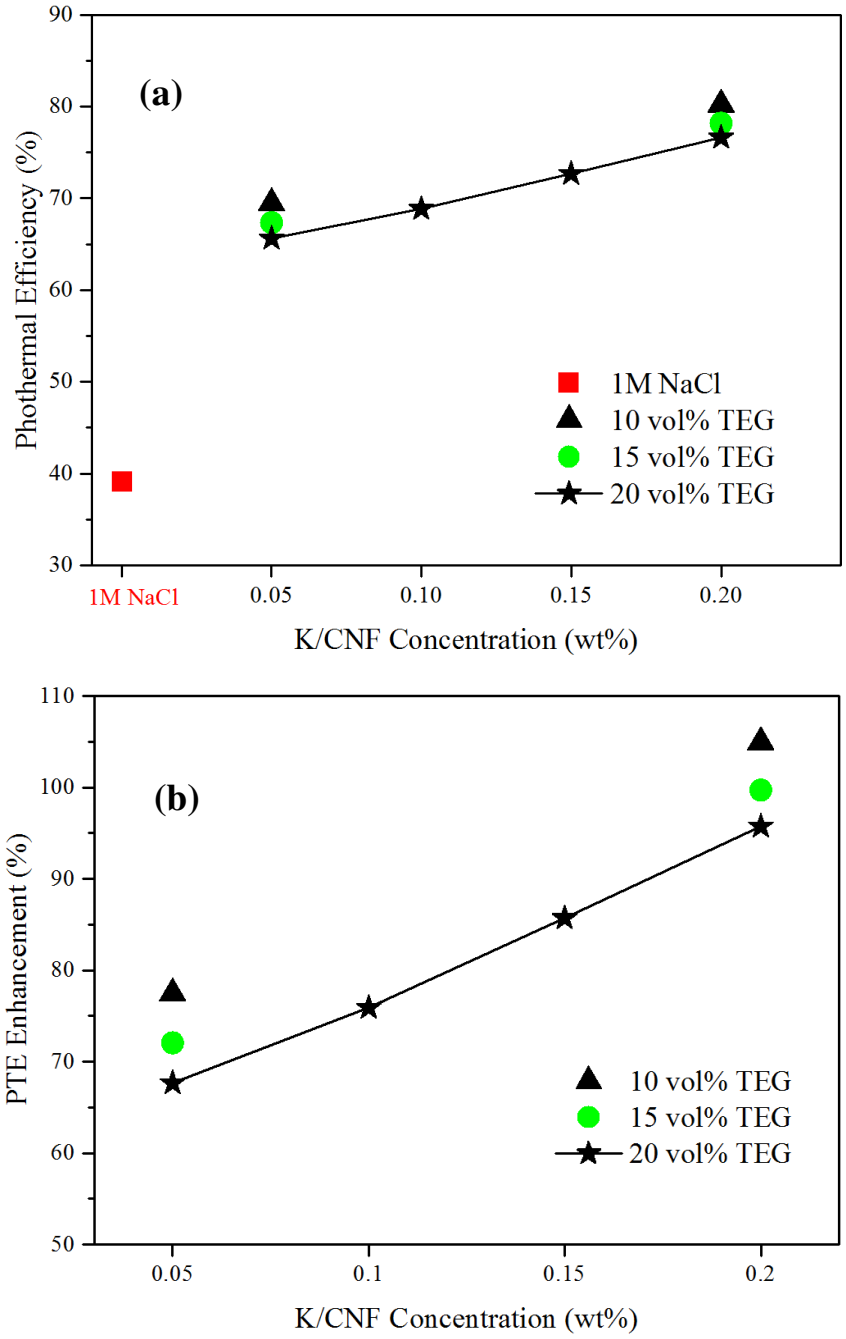

Fig. 12 (a) Photothermal efficiency of NDS at various concentrations of K/CNF and TEG as a result of exposure to radiation flux of 10 suns for 20 min and (b) enhancement in photothermal efficiency of NDS

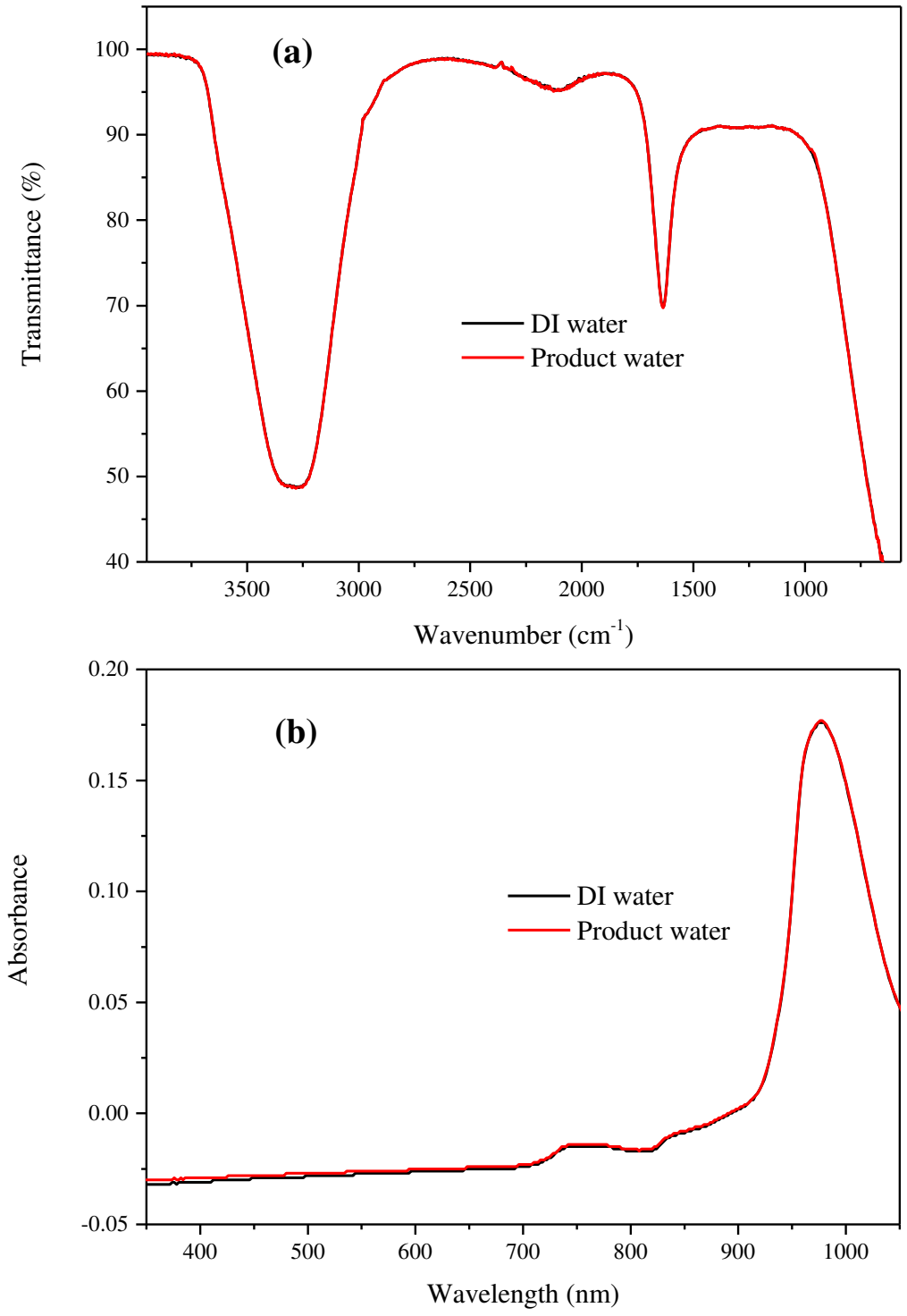

Fig. 13 Spectra of the product water and DI water from (a) FTIR and (b) UV-VIS spectrometer